# Primordial features due to a step in the inflaton potential

**Dhiraj Kumar Hazra[1+], Moumita Aich[2†], Rajeev Kumar Jain[3*], L. Sriramkumar[1‡] and Tarun Souradeep[2§]**

[1]Harish-Chandra Research Institute, Chhatnag Road, Jhunsi, Allahabad 211 019, India.

[2]IUCAA, Post Bag 4, Ganeshkhind, Pune 411 007, India.

[3]Department of Theoretical Physics, University of Geneva, 24 Quai Ernest-Ansermet, CH-1211, Geneva 4, Switzerland.

E-mail: [+]dhiraj@hri.res.in, [†]moumita@iucaa.ernet.in, [*]rajeev.jain@unige.ch, [‡]sriram@hri.res.in, [§]tarun@iucaa.ernet.in

**Abstract.** Certain oscillatory features in the primordial scalar power spectrum are known to provide a better fit to the outliers in the cosmic microwave background data near the multipole moments of $\ell = 22$ and 40. These features are usually generated by introducing a step in the popular, quadratic potential describing the canonical scalar field. Such a model will be ruled out, if the tensors remain undetected at a level corresponding to a tensor-to-scalar ratio of, say, $r \simeq 0.1$. In this work, in addition to the popular quadratic potential, we investigate the effects of the step in a small field model and a tachyon model. With possible applications to future datasets (such as PLANCK) in mind, we evaluate the tensor power spectrum exactly, and include its contribution in our analysis. We compare the models with the WMAP (five as well as seven-year), the QUaD and the ACBAR data. As expected, a step at a particular location and of a suitable magnitude and width is found to improve the fit to the outliers (near $\ell = 22$ and 40) in all these cases. We point out that, if the tensors prove to be small (say, $r \lesssim 0.01$), the quadratic potential and the tachyon model will cease to be viable, and more attention will need to be paid to examples such as the small field models.

PACS numbers: 98.80.Cq, 98.70.Vc, 04.30.-w

## 1. Outliers, inflationary models with a step, and tensors

Inflation continues to remain the most promising paradigm for describing the origin of the perturbations in the early universe. It has been performing remarkably well against the observational data, and the challenge before the other competing scenarios is to match the simplicity and efficiency of inflation. Many models of inflation lead to an epoch of slow roll lasting for, say, 50-60 e-folds, as is required to resolve the horizon problem. It is well known that slow roll inflation leads to a featureless, nearly scale invariant, power law, primordial scalar spectrum. Such a spectrum, along with the assumption of a spatially flat, concordant ΛCDM background cosmological model, provides a good fit to the recent observations of the anisotropies in the Cosmic Microwave Background (CMB) by different missions such as the Wilkinson Microwave Anisotropy Probe (WMAP) [1, 2], the QUEST at DASI (QUaD) [3], and the Arcminute Cosmology Bolometer Array Receiver (ACBAR) [4].

The efficacy of the inflationary scenario also seems to be responsible for an important drawback. Though, as a paradigm, inflation can be considered to be a success, it would be fair to say that we are rather far from converging on a specific model or even a class of models of inflation. There exist a plethora of inflationary models that remain consistent with the data. We mentioned above that a nearly scale invariant, power law, scalar spectrum fits the observations of the anisotropies in the CMB quite well. However, there exist a few data points at the lower multipoles—notably, at the quadrapole ($\ell = 2$) and near the multipole moments of $\ell = 22$ and 40—which lie outside the cosmic variance associated with the power law primordial spectrum. Needless to add, statistically, a few outliers in a thousand or so data points can always be expected. These outliers were noticed in the WMAP first-year data, and they continue to be present even in the most recent, seven-year data, making them unlikely to be artifacts of data analysis. It is possible that they actually indicate certain non-trivial inflationary dynamics. In that case, these outliers are important from the phenomenological perspective of attempting to constrain the models from the data, because only a more restricted class of inflationary models can be expected to provide an improved fit to these outliers. Therefore, it is a worthwhile exercise to systematically explore models that lead to specific deviations from the standard power law, inflationary perturbation spectrum, and also provide an improved fit to the data.

Various efforts towards a model independent reconstruction of the primordial spectrum from the observed pattern of the CMB anisotropies seem to indicate the presence of certain features in the spectrum [5]. In particular, a burst of oscillations in the primordial spectrum seems to provide a better fit to the CMB angular power spectrum near the multipole moments of $\ell = 22$ and 40. Generating these oscillations requires a short period of deviation from slow roll inflation [6, 7], and such a departure has often been achieved by introducing a small step in the popular, quadratic potential describing the canonical scalar field (see Refs. [8, 9, 10]; for a discussion on other models, see, for instance, Refs. [11, 12]). At the cost of three additional parameters

which characterize the location, the height and the width of the step, it has been found that this model provides a considerably better fit to the CMB data with the least squares parameter $\chi^2_{\rm eff}$ typically improving by about 7, when compared to the nearly scale invariant spectrum that would have resulted in the absence of the step [9, 10]. But, such a chaotic inflation model leads to a reasonable amount of tensors, and these models will be ruled out if tensors are not detected corresponding to a tensor-to-scalar ratio of, say, $r \simeq 0.1$.

Our aims in this paper are twofold. Firstly, we wish to examine whether, with the introduction of a step, other inflationary models too perform equally well against the CMB data, as the quadratic potential does. Secondly, we would also like to consider a model that leads to a tensor-to-scalar ratio of $r < 0.1$, so that suitable alternative models exist if the tensor contribution turns out to be smaller. Motivated by these considerations, apart from revisiting the popular quadratic potential, we shall investigate the effects of the step in a small field model (in this context, see, for example, Ref. [13]) and a tachyon model [14]. Also, with possible applications to future datasets in mind (such as the ongoing PLANCK mission [15]), we shall evaluate the tensor power spectrum exactly, and include its contribution in our analysis. We shall compare the models with the CMB data from the WMAP, the QUaD and the ACBAR missions. We shall consider the five as well as the seven-year WMAP data [1, 2], the QUaD June 2009 data [3] and the ACBAR 2008 data [4] to arrive at the observational constraints on the inflationary parameters. We find that, as one may expect, a step at a suitable location and of a certain magnitude and width improves the fit to the outliers (near $\ell = 22$ and 40) in all the cases. We point out that, if the amplitude of the tensors prove to be small, the quadratic potential and the tachyon model will become inviable, and we will have to turn our attention to examples such as the small field models.

The remainder of this paper is organized as follows. In the following section, we shall outline the different inflationary models that we shall be considering in this work. In Section 3, we shall discuss the methodology that we adopt for comparing the inflationary models with the data, the datasets that we use for our analysis, and the priors on the various parameters that we work with. In Section 4, we shall present the results of our comparison of the theoretical CMB angular power spectra that arise from the various models with the WMAP five-year as well as seven-year data, the QUaD and the ACBAR data. We shall tabulate and also illustrate the constraints that we obtain on the background cosmological parameters and the parameters describing the inflationary models. We shall also explicitly show that the models with the step perform better against the data because of the fact that they lead to an improvement in the fit to the outliers around $\ell = 22$ and 40. In Section 5, we shall illustrate the scalar power spectra and the CMB angular power spectra corresponding to the best fit values of the parameters of some of the models that we consider. Finally, in Section 6, we shall close with a brief summary, and a few comments on certain implications of our results. The appendix contains some details concerning the numerical evaluation of the inflationary scalar and tensor power spectra, and the numerical precision of our computation.

Note that we shall work in units such that $\hbar = c = (8\,\pi\,G) = 1$. Moreover, we shall assume the background cosmological model to be the standard, spatially flat, ΛCDM model.

## 2. The inflationary models of our interest

In this section, we shall list the different inflationary models that we shall consider, and briefly outline the parameters involved in each of these cases.

### *2.1. The conventional, power law case*

When the tensor perturbations are also taken into account, the power law, scalar and tensor spectra are written as (see, for example, Refs. [16, 17])

$$\mathcal{P}_{_{\rm S}}(k) = A_{_{\rm S}}\left(\frac{k}{k_0}\right)^{n_{_{\rm S}}-1} \quad \text{and} \quad \mathcal{P}_{_{\rm T}}(k) = A_{_{\rm T}}\left(\frac{k}{k_0}\right)^{n_{_{\rm T}}}, \tag{1}$$

respectively. The quantities $A_{_{\rm S}}$ and $A_{_{\rm T}}$ denote the amplitude of the scalar and tensor spectra, while $n_{_{\rm S}}$ and $n_{_{\rm T}}$ denote the corresponding spectral indices. The quantity $k_0$ is the pivot scale at which the amplitudes of the power spectra are quoted. It is this power law case that will act as our reference model with respect to which we shall compare the performance of the other models against the data.

Given the scalar and tensor spectra, i.e. $\mathcal{P}_{_{\rm S}}(k)$ and $\mathcal{P}_{_{\rm T}}(k)$, the tensor-to-scalar ratio is defined as

$$r(k) = \frac{\mathcal{P}_{_{\rm T}}(k)}{\mathcal{P}_{_{\rm S}}(k)}. \tag{2}$$

When comparing the power law case with the observations, it is the tensor-to-scalar ratio $r$ that is usually considered instead of the tensor amplitude $A_{_{\rm T}}$. Often, the following slow roll consistency condition is further assumed (see, for instance, Refs. [1, 2, 3, 4])

$$r = -8\,n_{_{\rm T}}, \tag{3}$$

so that the power law case is basically described by the three parameters $A_{_{\rm S}}$, $n_{_{\rm S}}$ and $r$. We should mention here that we shall *not* impose the above consistency condition while comparing the power law case with the data, and we shall work with all the four parameters $A_{_{\rm S}}$, $n_{_{\rm S}}$, $r$ and $n_{_{\rm T}}$.

### *2.2. Canonical scalar field models*

We shall work with two types of canonical scalar field models. We shall firstly revisit the large field, quadratic model described by the potential

$$V(\phi) = \frac{1}{2}\,m^2\,\phi^2, \tag{4}$$

where $m$ represents the mass of the inflaton. The parameter $m$ is essentially determined by the amplitude of the scalar power spectrum. To achieve the required number, say, 60 e-folds of inflation, in such a model, the field has to start at a suitably large value

(in units of the Planck mass). The field rolls down the potential, and inflation ends as the field nears the minimum of the potential (see, for instance, Refs. [16, 17]).

In addition, we shall consider the small field model governed by the potential

$$V(\phi) = V_0 \left[1 - (\phi/\mu)^p\right]. \tag{5}$$

The field starts at small values in such models, and inflation is terminated naturally as the field approaches the value $\mu$. As is well known (and, as we shall also discuss), the quadratic potential Eq. (4) leads to a tensor-to-scalar ratio of $r \simeq 0.1$ [10]. The small field model Eq. (5) can lead to a smaller tensor-to-scalar ratio for suitable values of $\mu$ and $p$ (in this context, see Ref. [13]). Also, when $p < 4$, the model is known to result in a substantial red tilt. We find that, if we choose $p = 4$ and $\mu = 15$, the model leads to a tilt that is consistent with observations, and a tensor-to-scalar ratio of $r \simeq 0.01$. So while comparing with the data, we shall work with these specific values of $p$ and $\mu$, and vary $V_0$.

### *2.3. Tachyon model*

Tachyonic inflationary potentials are usually written in terms of two parameters, say, $\lambda$ and $\phi_*$, in the following form [14]:

$$V(\phi) = \lambda\, V_1(\phi/\phi_*), \tag{6}$$

where $V_1(\phi/\phi_*)$ is a function which has a maximum at the origin and vanishes as $\phi \to \infty$. The tachyon model that we shall consider is described by the potential

$$V(\phi) = \frac{\lambda}{\cosh\left(\phi/\phi_*\right)}. \tag{7}$$

In such a potential, inflation typically occurs around $\phi \simeq \phi_*$. The field rolls down the potential, and inflation ends at suitably large values of the field. It is found that the quantity $(\lambda\,\phi_*^2)$ has to be much larger than unity to ensure that inflation lasts for a sufficiently long time [14]. We find that the amplitude of the scalar perturbations is more sensitive to $\phi_*$ than $\lambda$. Hence, while comparing with the data, we fix the value of $\lambda$, and vary $\phi_*$. We shall set $\lambda = 8.9 \times 10^{-4}$. We shall then choose the priors on $\phi_*$ such that $(\lambda\,\phi_*^2)$ is relatively large in order to achieve the required duration of slow roll inflation.

In fact, we have also considered the following phenomenological model [14]:

$$V(\phi) = \frac{\lambda}{1 + (\phi/\phi_*)^4}. \tag{8}$$

We have compared this model with the WMAP five-year, the QUaD and the ACBAR data sets. The model generically seems to lead to a larger red tilt and, as a result, it does not perform as well against the data as the other models. Therefore, we have not compared it with the WMAP seven-year data. So, we shall not present the results for this case (say, the constraints on the potential parameters), but restrict ourselves to brief comments on its performance at one or two places.

### *2.4. Introduction of the step*

Given a potential, say, $V(\phi)$, we shall introduce the step by *multiplying* the potential by the following function:

$$V_{\rm step}(\phi) = \left[1 + \alpha \, \tanh\left(\frac{\phi - \phi_0}{\Delta\phi}\right)\right], \tag{9}$$

as is often done in the literature [8, 9, 10]. It should be pointed out that the quantity $\alpha$ is positive in the case of the quadratic potential Eq. (4), whereas it is negative in the cases of the small field model Eq. (5), and the tachyon models Eqs. (7) and (8). Evidently, $\alpha$ denotes the height of the step, $\phi_0$ its location, and $\Delta\phi$ its width. When comparing with the data, in addition to the potential parameters, we shall vary these three parameters, along with the background cosmological parameters, to arrive at the observational constraints.

## 3. Methodology, datasets, and priors

We evaluate the inflationary power spectra numerically. In addition to the scalar power spectrum, we evaluate the tensor spectrum exactly, and include it in our analysis. In Appendix A, we have discussed, in some detail, the procedures we adopt to compute the primordial scalar and tensor spectra. In order to arrive at the constraints on the various background cosmological parameters and the parameters describing the inflaton potential, we perform a Markov Chain Monte-Carlo sampling of the parameter space. To do so, we make use of the publicly available CosmoMC package [18, 19], which in turn uses the CMB anisotropy code CAMB [20, 21] to generate the CMB angular power spectra from the primordial scalar and tensor spectra. For our analysis, we consider the following CMB datasets: the WMAP five-year [1] and seven-year data [2], the QUaD June 2009 data [3], and the the ACBAR 2008 data [4]. We have separately compared the models with the WMAP five-year and seven-year data. We have also compared the models with the WMAP five-year data along with the QUaD data, and with the QUaD as well as the ACBAR data. We have used the October 2009 version of CosmoMC (and CAMB) while comparing with the WMAP five-year and the QUaD and the ACBAR datasets. When comparing with the WMAP seven-year data, we have made use of the more recent version (i.e. the January 2010 version) of CosmoMC and CAMB.

In our analysis, we take gravitational lensing into account. Note that, to generate highly accurate lensed CMB spectra, CAMB requires $\ell_{\rm max\ scalar} \simeq (\ell_{\rm max} + 500)$, where $\ell_{\rm max}$ is, say, the largest multipole moment for which the data is available. The WMAP data is available up to $\ell \simeq 1200$, the QUaD data goes up to $\ell \simeq 2000$, while the ACBAR data is available up to $\ell \simeq 2700$. So, we set $\ell_{\rm max\ scalar} = 2500$ when dealing with the WMAP and the QUaD datasets and, when we include the ACBAR data, we set $\ell_{\rm max\ scalar} = 3300$. Since the datasets involve rather large multipole moments (say, $\ell \gtrsim 1000$), we also take into account the Sunyaev-Zeldovich effect, and marginalize over the $A_{\rm sz}$ parameter. For the power law case, we set the pivot scale to be $k_0 = 0.05$ Mpc$^{-1}$

[cf. Eq. (1)]. We have made use of the publicly available WMAP likelihood code from the LAMBDA web-site [22] to determine the performance of the models against the data. Lastly, we should add that we have used the Gibbs option (for the CMB $TT$ spectrum at the low multipoles) in the WMAP likelihood code to evaluate the least square parameter $\chi^2_{\rm eff}$.

As we had mentioned earlier, we incorporate the tensor perturbations in our analysis. Recall that, in the power law case, when the consistency condition Eq. (3) is not imposed, the tensor power spectrum is described in terms of the tensor-to-scalar ratio $r$ and the tensor spectral index $n_{_{\rm T}}$. They need to be specified along with the scalar amplitude $A_{_{\rm S}}$ and the corresponding spectral index $n_{_{\rm S}}$, in order to completely describe the primordial spectra. We should emphasize that, in the other inflationary models, once the parameters that govern the potential have been specified, no further parameters are required to describe the tensor power spectrum. The potential parameters determine the amplitude and shape of *both* the scalar and the tensor spectra.

We shall set the Gelman and Rubin parameter $|R-1|$ to be 0.1 for convergence. We find that, for the models that we consider, there is no substantial improvement in the fit if we choose a smaller value of $|R-1|$. For example, for the case of the quadratic potential Eq. (4), we find that decreasing $|R-1|$ from 0.1 to 0.05 improves $\chi^2_{\rm eff}$ by about 0.04. We believe that choosing $|R-1| = 0.1$ for convergence suffices for our analysis.

In Table 1, we have listed the priors that we work with for the four parameters that are usually used to describe the background, spatially flat, ΛCDM model. Table 2 contains the priors that we choose on the different parameters which describe the various inflationary models that we consider.

| Background parameter | Lower limit | Upper limit |
|---|---|---|
| $\Omega_{\rm b}\, h^2$ | 0.005 | 0.1 |
| $\Omega_{\rm c}\, h^2$ | 0.01 | 0.99 |
| $\theta$ | 0.5 | 10.0 |
| $\tau$ | 0.01 | 0.8 |

**Table 1.** The priors on the four parameters that describe the background, spatially flat, ΛCDM model. The quantities $(\Omega_{\rm b}\, h^2)$ and $(\Omega_{\rm c}\, h^2)$ describe the baryon and CDM densities (with $h$ being related to the Hubble parameter), $\theta$ is the ratio of the sound horizon to the angular diameter distance at decoupling, while $\tau$ is the optical depth to reionization. We should mention that we keep the same priors on the background parameters for all the models and datasets that we consider in our analysis.

## 4. Bounds on the background cosmology and the inflationary parameters

In this section, we shall present the results of our analysis. As we mentioned above, we have separately compared the models with the WMAP five-year and seven-year data.

| Models | Parameter | Lower limit | Upper limit |
|---|---|---|---|
| Power law case | $\ln\left[10^{10}\,A_{\rm S}\right]$ | 2.7 | 4.0 |
| | $n_{\rm S}$ | 0.5 | 1.5 |
| | $r$ | 0.0 | 1.0 |
| | $n_{\rm T}$ | $-0.5$ | 0.5 |
| Quadratic model | $\ln\left[10^{10}\,m^2\right]$ | $-0.77$ | $-0.58$ |
| Quadratic model with a step | $\ln\left[10^{10}\,m^2\right]$ | $-0.77$ | $-0.58$ |
| | $\alpha$ | $1.3\times10^{-3}$ | $1.7\times10^{-3}$ |
| | $\phi_0$ | 13.0 | 15.0 |
| | $\Delta\phi$ | 0.015 | 0.03 |
| Small field model | $\ln\left[10^{10}\,V_0\right]$ | 1.50 | 1.86 |
| Small field model with a step | $\ln\left[10^{10}\,V_0\right]$ | 1.50 | 1.86 |
| | $-\alpha$ | $1.0\times10^{-4}$ | $2.0\times10^{-4}$ |
| | $\phi_0$ | 7.8 | 8.1 |
| | $\Delta\phi$ | $5.0\times10^{-3}$ | $1.0\times10^{-2}$ |
| Tachyon model | $\ln\left[10^{10}\,\phi_*\right]$ | 34.506 | 34.518 |
| Tachyon model with a step | $\ln\left[10^{10}\,\phi_*\right]$ | 34.506 | 34.518 |
| | $-\alpha$ | $1.3\times10^{-3}$ | $1.9\times10^{-3}$ |
| | $\phi_0$ | $7.81\times10^{5}$ | $7.83\times10^{5}$ |
| | $\Delta\phi$ | 340 | 410 |

**Table 2.** The priors on the various parameters that describe the primordial spectrum in the power law case, and the inflationary potential in all the other cases. We work with these priors when comparing the models with all the datasets.

We have also compared the models with the WMAP five-year data along with the QUaD data, and with the QUaD as well as the ACBAR data. We shall tabulate below the constraints that we arrive at on the various background and inflationary parameters in these different instances. We shall list the mean values, the 1-$\sigma$ deviations, and the best fit values that we arrive at for the power law case and for the inflationary models with the step. We shall also illustrate the behavior of the one-dimensional likelihoods for the background parameters in the case of the small field model with the step. Moreover, we shall plot the one-dimensional likelihoods of the three parameters (i.e. $\alpha$, $\phi_0$ and $\Delta\phi$) that describe the step for all the three inflationary models that we have considered, viz. the quadratic potential Eq. (4), the small field model Eq. (5) and the tachyon model Eq. (7). Further, we shall also provide the least squares parameter $\chi^2_{\rm eff}$ in all the cases.

### *4.1. The mean values, the* 1-$\sigma$ *deviations, and the best fit values*

In Tables 3, 4, 5 and 6, we have listed the mean values, the 1-$\sigma$ deviations, as well as the best fit values for the various parameters for the different models. These tables contain the results that we arrive at upon comparing the models with the WMAP five-year (denoted as WMAP-5), the QUaD as well as the ACBAR data sets. Note that we have only presented the results for the power law case, and when the step Eq. (9) has been introduced in the quadratic potential Eq. (4), the small field model Eq. (5) and the tachyon model Eq. (7). We find that the values we have obtained upon comparing the

power law case with the WMAP-five year and the QUaD and the ACBAR data match well with the results quoted by the WMAP [1] and the QUaD teams [3]. Also, the results for the quadratic potential with the step agree well with the results quoted in the recent work [10].

| Datasets | WMAP-5 | | WMAP-5 + QUaD | | WMAP-5 + QUaD + ACBAR | |
|---|---|---|---|---|---|---|
| Parameters | Mean & 1-$\sigma$ | Best fit | Mean & 1-$\sigma$ | Best fit | Mean & 1-$\sigma$ | Best fit |
| $\Omega_{\rm b}\,h^2$ | $0.0234^{+0.0007}_{-0.0007}$ | 0.0230 | $0.0234^{+0.0007}_{-0.0007}$ | 0.0230 | $0.0234^{+0.0007}_{-0.0007}$ | 0.0228 |
| $\Omega_{\rm c}\,h^2$ | $0.1042^{+0.0066}_{-0.0068}$ | 0.1069 | $0.1022^{+0.0071}_{-0.0072}$ | 0.1037 | $0.1036^{+0.0062}_{-0.0062}$ | 0.1097 |
| $\theta$ | $1.042^{+0.003}_{-0.003}$ | 1.040 | $1.042^{+0.003}_{-0.003}$ | 1.040 | $1.043^{+0.003}_{-0.003}$ | 1.042 |
| $\tau$ | $0.0933^{+0.0074}_{-0.0090}$ | 0.0937 | $0.0960^{+0.0077}_{-0.0091}$ | 0.0839 | $0.0937^{+0.0075}_{-0.0085}$ | 0.0861 |
| $\ln\left[10^{10}\,A_{\rm S}\right]$ | $3.060^{+0.042}_{-0.044}$ | 3.057 | $3.057^{+0.040}_{-0.040}$ | 3.027 | $3.058^{+0.041}_{-0.039}$ | 3.058 |
| $n_{\rm S}$ | $0.9857^{+0.0208}_{-0.0208}$ | 0.9658 | $0.9880^{+0.0209}_{-0.0207}$ | 0.9704 | $0.9840^{+0.0189}_{-0.0191}$ | 0.9625 |
| $r$ | $0.3740^{+0.1163}_{-0.3740}$ | 0.1072 | $0.3976^{+0.1424}_{-0.3976}$ | 0.4420 | $0.3646^{+0.1175}_{-0.3646}$ | 0.0741 |
| $n_{\rm T}$ | $0.2565^{+0.2430}_{-0.1939}$ | 0.2881 | $0.2401^{+0.2594}_{-0.2082}$ | 0.4857 | $0.2620^{+0.2376}_{-0.1763}$ | 0.4072 |
| $\Omega_\Lambda$ | $0.7720^{+0.0310}_{-0.0304}$ | 0.7576 | $0.7823^{+0.0312}_{-0.0319}$ | 0.7715 | $0.7776^{+0.0287}_{-0.0289}$ | 0.7482 |
| Age/Gyr | $13.55^{+0.16}_{-0.16}$ | 13.65 | $13.51^{+0.15}_{-0.15}$ | 13.63 | $13.51^{+0.14}_{-0.14}$ | 13.64 |
| $\Omega_{\rm m}$ | $0.2280^{+0.0304}_{-0.0310}$ | 0.2424 | $0.2177^{+0.0319}_{-0.0312}$ | 0.2285 | $0.2224^{+0.0289}_{-0.0287}$ | 0.2517 |
| $z_{\rm re}$ | $10.50^{+1.32}_{-1.40}$ | 10.75 | $10.65^{+1.32}_{-1.32}$ | 9.893 | $10.53^{+1.31}_{-1.31}$ | 10.27 |
| $\rm H_0$ | $75.19^{+3.33}_{-3.33}$ | 73.21 | $76.40^{+3.61}_{-3.71}$ | 74.47 | $75.91^{+3.30}_{-3.21}$ | 72.53 |

**Table 3.** The mean values, the 1-$\sigma$ deviations, and the best fit values that we arrive at upon comparing the power law primordial spectra Eq. (1) with the WMAP five-year, the QUaD and the ACBAR data sets. The first eight rows correspond to the parameters that describe the background parameters and the power law primordial spectra, whereas the remaining ones are the derived values. We should point out that the best fit values that we have arrived at on using the WMAP five-year data match well with the values quoted by the WMAP team [1]. Similarly, we find that the bounds we have obtained upon comparing with the WMAP-five year and the QUaD and the ACBAR data are in good agreement with the results arrived at by, say, the QUaD team [3]. Note that, while the WMAP team [1] had worked with the pivot point of $k_0 = 0.002$ Mpc$^{-1}$, the QUaD team had set the pivot scale to be $k_0 = 0.05$ Mpc$^{-1}$, as we do. However, we should clarify that, whereas the WMAP and the QUaD teams had imposed the consistency condition Eq. (3), we have not done so in our analysis.

In Table 7, we have presented the bounds for the power law case that we obtain upon comparison with the WMAP seven-year data. Again, we should mention that the results listed in Table 7 agree well with the ones listed in the recent WMAP paper [2]. Tables 8 and 9 contain the constraints from the WMAP seven-year data on the parameters describing the three inflationary models of our interest without and with the step, respectively.

### *4.2. The one-dimensional likelihoods and the joint two-dimensional constraints*

In Figure 1, as an illustration, we have plotted the one-dimensional likelihoods for the background parameters in the case of the small field model with the step. In Figure 2, we have plotted the likelihood curves for the parameters that characterize the step in all the three inflationary models that we have considered. We find that, while the data constrain the location of the step quite well in the canonical scalar field models, but

| Datasets | WMAP-5 | | WMAP-5 + QUaD | | WMAP-5 + QUaD + ACBAR | |
|---|---|---|---|---|---|---|
| Parameters | Mean & 1-$\sigma$ | Best fit | Mean & 1-$\sigma$ | Best fit | Mean & 1-$\sigma$ | Best fit |
| $\Omega_{\rm b}\,h^2$ | $0.0226^{+0.0004}_{-0.0004}$ | 0.0227 | $0.0226^{+0.0003}_{-0.0003}$ | 0.0227 | $0.0227^{+0.0003}_{-0.0003}$ | 0.0229 |
| $\Omega_{\rm c}\,h^2$ | $0.1104^{+0.0062}_{-0.0064}$ | 0.1085 | $0.1092^{+0.0057}_{-0.0056}$ | 0.1084 | $0.1098^{+0.0050}_{-0.0049}$ | 0.1097 |
| $\theta$ | $1.040^{+0.002}_{-0.002}$ | 1.040 | $1.041^{+0.002}_{-0.002}$ | 1.041 | $1.042^{+0.002}_{-0.002}$ | 1.042 |
| $\tau$ | $0.0861^{+0.0066}_{-0.0071}$ | 0.0896 | $0.0870^{+0.0067}_{-0.0073}$ | 0.0890 | $0.0861^{+0.0067}_{-0.0071}$ | 0.0859 |
| $\ln\left[10^{10}\,m^2\right]$ | $-0.6809^{+0.0369}_{-0.0375}$ | $-0.6848$ | $-0.6835^{+0.0348}_{-0.0352}$ | $-0.6834$ | $-0.6823^{+0.0342}_{-0.0345}$ | $-0.6850$ |
| $\alpha \times 10^4$ | $14.86^{+1.39}_{-1.85}$ | 15.04 | $14.84^{+1.32}_{-1.83}$ | 15.45 | $14.80^{+1.37}_{-1.79}$ | 15.68 |
| $\phi_0$ | $14.67^{+0.01}_{-0.01}$ | 14.67 | $14.67^{+0.01}_{-0.01}$ | 14.67 | $14.67^{+0.01}_{-0.01}$ | 14.67 |
| $\Delta\phi$ | $0.0250^{+0.0050}_{-0.0037}$ | 0.0271 | $0.0249^{+0.0051}_{-0.0038}$ | 0.0264 | $0.0251^{+0.0049}_{-0.0036}$ | 0.0282 |
| $\alpha/\Delta\phi$ | $0.0606^{+0.0097}_{-0.0092}$ | 0.0555 | $0.0608^{+0.0095}_{-0.0092}$ | 0.0585 | $0.0601^{+0.0091}_{-0.0091}$ | 0.0556 |
| $\Omega_\Lambda$ | $0.7374^{+0.0289}_{-0.0283}$ | 0.7467 | $0.7459^{+0.0252}_{-0.0261}$ | 0.7504 | $0.7459^{+0.0225}_{-0.0223}$ | 0.7486 |
| Age/Gyr | $13.72^{+0.08}_{-0.08}$ | 13.72 | $13.68^{+0.08}_{-0.08}$ | 13.68 | $13.65^{+0.07}_{-0.07}$ | 13.62 |
| $\Omega_{\rm m}$ | $0.2626^{+0.0283}_{-0.0289}$ | 0.2533 | $0.2541^{+0.0261}_{-0.0252}$ | 0.2496 | $0.2541^{+0.0223}_{-0.0225}$ | 0.2514 |
| $z_{\rm re}$ | $10.29^{+1.28}_{-1.25}$ | 10.56 | $10.33^{+1.25}_{-1.25}$ | 10.51 | $10.27^{+1.27}_{-1.26}$ | 10.22 |
| $\rm H_0$ | $71.39^{+2.26}_{-2.27}$ | 71.98 | $72.22^{+2.11}_{-2.19}$ | 72.46 | $72.35^{+1.92}_{-1.90}$ | 72.61 |

**Table 4.** The mean values, the 1-$\sigma$ deviations and the best fit values for the various input and derived parameters corresponding to the quadratic potential Eq. (4) with the step Eq. (9). We should point out that the best fit values for the parameters that we have arrived at with the WMAP five-year data above are in good agreement with the results quoted in the recent work [10].

| Datasets | WMAP-5 | | WMAP-5 + QUaD | | WMAP-5 + QUaD + ACBAR | |
|---|---|---|---|---|---|---|
| Parameters | Mean & 1-$\sigma$ | Best fit | Mean & 1-$\sigma$ | Best fit | Mean & 1-$\sigma$ | Best fit |
| $\Omega_{\rm b}\,h^2$ | $0.0226^{+0.0004}_{-0.0004}$ | 0.0228 | $0.0227^{+0.0003}_{-0.0003}$ | 0.0229 | $0.0227^{+0.0003}_{-0.0003}$ | 0.0229 |
| $\Omega_{\rm c}\,h^2$ | $0.1101^{+0.0064}_{-0.0064}$ | 0.1081 | $0.1092^{+0.0057}_{-0.0057}$ | 0.1079 | $0.1095^{+0.0051}_{-0.0051}$ | 0.1097 |
| $\theta$ | $1.040^{+0.003}_{-0.003}$ | 1.040 | $1.041^{+0.002}_{-0.002}$ | 1.040 | $1.042^{+0.002}_{-0.002}$ | 1.042 |
| $\tau$ | $0.0864^{+0.0069}_{-0.0075}$ | 0.0868 | $0.0877^{+0.0068}_{-0.0071}$ | 0.0915 | $0.0884^{+0.0071}_{-0.0075}$ | 0.0846 |
| $\ln\left[10^{10}\,V_0\right]$ | $1.697^{+0.038}_{-0.037}$ | 1.687 | $1.696^{+0.036}_{-0.036}$ | 1.700 | $1.698^{+0.035}_{-0.035}$ | 1.690 |
| $-\alpha \times 10^3$ | $0.1417^{+0.0324}_{-0.0417}$ | 0.1114 | $0.1411^{+0.0333}_{-0.0411}$ | 0.1266 | $0.1409^{+0.0322}_{-0.0408}$ | 0.1121 |
| $\phi_0$ | $7.885^{+0.005}_{-0.002}$ | 7.887 | $7.886^{+0.004}_{-0.003}$ | 7.888 | $7.887^{+0.003}_{-0.004}$ | 7.890 |
| $\Delta\phi$ | $0.0080^{+0.0019}_{-0.0014}$ | 0.0085 | $0.0081^{+0.0014}_{-0.0014}$ | 0.0084 | $0.0080^{+0.0019}_{-0.0014}$ | 0.0080 |
| $-(\alpha/\Delta\phi)$ | $0.0181^{+0.0039}_{-0.0041}$ | 0.0176 | $0.0178^{+0.0038}_{-0.0041}$ | 0.0178 | $0.0178^{+0.0038}_{-0.0040}$ | 0.0178 |
| $\Omega_\Lambda$ | $0.7398^{+0.0284}_{-0.0286}$ | 0.7495 | $0.7464^{+0.0256}_{-0.0256}$ | 0.7529 | $0.7478^{+0.0229}_{-0.0231}$ | 0.7478 |
| Age/Gyr | $13.71^{+0.09}_{-0.09}$ | 13.70 | $13.68^{+0.08}_{-0.08}$ | 13.66 | $13.64^{+0.07}_{-0.07}$ | 13.63 |
| $\Omega_{\rm m}$ | $0.2602^{+0.0286}_{-0.0284}$ | 0.2505 | $0.2536^{+0.0256}_{-0.0256}$ | 0.2471 | $0.2522^{+0.0231}_{-0.0229}$ | 0.2522 |
| $z_{\rm re}$ | $10.30^{+1.31}_{-1.29}$ | 10.29 | $10.38^{+1.26}_{-1.26}$ | 10.63 | $10.43^{+1.28}_{-1.29}$ | 10.10 |
| $\rm H_0$ | $71.62^{+2.26}_{-2.27}$ | 72.28 | $72.29^{+2.14}_{-2.16}$ | 72.74 | $72.56^{+1.96}_{-1.98}$ | 72.50 |

**Table 5.** The mean values, the 1-$\sigma$ deviations and the best fit values for the various input and derived parameters corresponding to the small field model Eq. (5) with a step.

the bounds on the height and the width of the step are not equally tight. In contrast, the bounds we have arrived at on the parameters of the tachyon model seem prior dominated.

Interestingly, though neither the height nor the width of the step are well bounded individually, we find that the data constrains the ratio of the two fairly tightly. In Figure 3, we have plotted the ratio $(\alpha/\Delta\phi)$ for all the three inflationary models of our interest. (Note that, in Figures 1–3, WMAP-7 refers to the WMAP seven-year data.) And, in Figure 4, we have plotted the joint two-dimensional likelihood distributions

| Datasets | WMAP-5 | | WMAP-5 + QUaD | | WMAP-5 + QUaD + ACBAR | |
|---|---|---|---|---|---|---|
| Parameters | Mean & 1-$\sigma$ | Best fit | Mean & 1-$\sigma$ | Best fit | Mean & 1-$\sigma$ | Best fit |
| $\Omega_{\rm b}\,h^2$ | $0.0227^{+0.0004}_{-0.0004}$ | 0.0226 | $0.0226^{+0.0004}_{-0.0004}$ | 0.0227 | $0.0227^{+0.0003}_{-0.0003}$ | 0.0229 |
| $\Omega_{\rm c}\,h^2$ | $0.1103^{+0.0048}_{-0.0052}$ | 0.1128 | $0.1100^{+0.0050}_{-0.0051}$ | 0.1109 | $0.1104^{+0.0046}_{-0.0046}$ | 0.1104 |
| $\theta$ | $1.040^{+0.003}_{-0.003}$ | 1.040 | $1.041^{+0.002}_{-0.002}$ | 1.041 | $1.042^{+0.002}_{-0.002}$ | 1.043 |
| $\tau$ | $0.0899^{+0.0049}_{-0.0046}$ | 0.0858 | $0.0914^{+0.0050}_{-0.0055}$ | 0.0910 | $0.0906^{+0.0046}_{-0.0049}$ | 0.0933 |
| $\ln\left[10^{10}\,\phi_*\right]$ | $34.511^{+0.004}_{-0.003}$ | 34.509 | $34.510^{+0.004}_{-0.003}$ | 34.508 | $34.510^{+0.004}_{-0.003}$ | 34.509 |
| $-\alpha$ | $0.0016^{+0.0002}_{-0.0003}$ | 0.0016 | $0.0016^{+0.0003}_{-0.0002}$ | 0.0017 | $0.0016^{+0.0002}_{-0.0002}$ | 0.0017 |
| $\phi_0 \times 10^{-6}$ | $0.7820^{+0.0005}_{-0.0004}$ | 0.7828 | $0.7820^{+0.0007}_{-0.0007}$ | 0.7820 | $0.7820^{+0.0007}_{-0.0007}$ | 0.7829 |
| $\Delta\phi$ | $371.0^{+20.5}_{-14.7}$ | 364.5 | $378.0^{+22.8}_{-24.3}$ | 395.9 | $374.9^{+23.1}_{-23.4}$ | 368.2 |
| $-(\alpha/\Delta\phi) \times 10^5$ | $0.4300^{+0.0581}_{-0.0561}$ | 0.4254 | $0.4268^{+0.0542}_{-0.0557}$ | 0.4218 | $0.4225^{+0.0538}_{-0.0537}$ | 0.4562 |
| $\Omega_\Lambda$ | $0.7393^{+0.0231}_{-0.0223}$ | 0.7272 | $0.7418^{+0.0234}_{-0.0226}$ | 0.7401 | $0.7435^{+0.0214}_{-0.0210}$ | 0.7465 |
| Age/Gyr | $13.70^{+0.08}_{-0.09}$ | 13.74 | $13.69^{+0.08}_{-0.08}$ | 13.68 | $13.65^{+0.07}_{-0.07}$ | 13.61 |
| $\Omega_{\rm m}$ | $0.2607^{+0.0223}_{-0.0231}$ | 0.2728 | $0.2582^{+0.0226}_{-0.0234}$ | 0.2599 | $0.2565^{+0.0210}_{-0.0214}$ | 0.2535 |
| $z_{\rm re}$ | $10.59^{+0.79}_{-0.78}$ | 10.38 | $10.73^{+0.82}_{-0.84}$ | 10.73 | $10.67^{+0.76}_{-0.75}$ | 10.86 |
| $\rm H_0$ | $71.57^{+1.85}_{-1.89}$ | 70.44 | $71.83^{+1.93}_{-1.93}$ | 71.69 | $72.15^{+1.82}_{-1.80}$ | 72.53 |

**Table 6.** The mean values, the 1-$\sigma$ deviations, and the best fit values for the various input and derived parameters corresponding to the tachyon model Eq. (7) with a step.

| Parameters | Mean & 1-$\sigma$ | Best fit |
|---|---|---|
| $\Omega_{\rm b}\,h^2$ | $0.0231^{+0.0007}_{-0.0007}$ | 0.0228 |
| $\Omega_{\rm c}\,h^2$ | $0.1063^{+0.0060}_{-0.0061}$ | 0.1087 |
| $\theta$ | $1.040^{+0.003}_{-0.003}$ | 1.040 |
| $\tau$ | $0.0913^{+0.0068}_{-0.0076}$ | 0.0927 |
| $\ln\left[10^{10}\,A_{\rm S}\right]$ | $3.073^{+0.034}_{-0.035}$ | 3.086 |
| $n_{\rm S}$ | $0.9857^{+0.0199}_{-0.0195}$ | 0.9798 |
| $r$ | $0.3319^{+0.1015}_{-0.3319}$ | 0.2902 |
| $n_{\rm T}$ | $0.2451^{+0.2546}_{-0.2095}$ | 0.4638 |
| $\Omega_\Lambda$ | $0.7592^{+0.0300}_{-0.0294}$ | 0.7467 |
| Age/Gyr | $13.63^{+0.16}_{-0.15}$ | 13.70 |
| $\Omega_{\rm m}$ | $0.2407^{+0.0294}_{-0.0300}$ | 0.2533 |
| $z_{\rm re}$ | $10.47^{+1.22}_{-1.21}$ | 10.78 |
| $\rm H_0$ | $73.65^{+3.11}_{-3.12}$ | 72.06 |

**Table 7.** The constraints on the input and derived parameters in the power law case obtained upon using the WMAP seven-year data. We should mention that these values match the ones quoted in the recent WMAP paper [2] rather well. However, we should point out that there is a difference in our choices of the pivot scales. Also, as we had mentioned earlier, we have chosen *not* to impose the consistency condition Eq. (3).

(from the WMAP seven-year data) of $\alpha$ and $\Delta\phi$ with the slope $(\alpha/\Delta\phi)$ for all the models. It is evident from these two figures that the ratio $(\alpha/\Delta\phi)$ is rather well constrained in all the three cases.

### *4.3. The effective least squares parameter* $\chi^2_{\rm eff}$

In Table 10, we have listed the least squares parameter $\chi^2_{\rm eff}$ for the different models and datasets of our interest. It is clear from the table that the presence of the step leads to a reduction in $\chi^2_{\rm eff}$ by about 7-9 in all the three inflationary models that we have considered. Also, note that such an improvement is achieved in all the datasets that we have compared the models with. We should mention that, with the introduction of

| Model | Quadratic potential | | Small field model | | Tachyon model | |
|---|---|---|---|---|---|---|
| Parameters | Mean & 1-$\sigma$ | Best fit | Mean & 1-$\sigma$ | Best fit | Mean & 1-$\sigma$ | Best fit |
| $\Omega_{\rm b}\,h^2$ | $0.0224^{+0.0003}_{-0.0003}$ | 0.0225 | $0.0224^{+0.0003}_{-0.0003}$ | 0.0225 | $0.0223^{+0.0003}_{-0.0003}$ | 0.0225 |
| $\Omega_{\rm c}\,h^2$ | $0.1112^{+0.0053}_{-0.0051}$ | 0.1103 | $0.1110^{+0.0055}_{-0.0055}$ | 0.1107 | $0.1108^{+0.0044}_{-0.0042}$ | 0.1107 |
| $\theta$ | $1.039^{+0.002}_{-0.002}$ | 1.039 | $1.039^{+0.002}_{-0.002}$ | 1.039 | $1.039^{+0.002}_{-0.002}$ | 1.039 |
| $\tau$ | $0.0862^{+0.0060}_{-0.0064}$ | 0.0881 | $0.0862^{+0.0059}_{-0.0068}$ | 0.0875 | $0.0847^{+0.0041}_{-0.0044}$ | 0.0827 |
| $\ln\left[10^{10}\,A_{\rm S}\right]$ | $-0.6709^{+0.0328}_{-0.0323}$ | $-0.6736$ | $1.708^{+0.033}_{-0.033}$ | 1.709 | $34.512^{+0.004}_{-0.004}$ | 34.515 |
| $\Omega_\Lambda$ | $0.7294^{+0.0247}_{-0.0250}$ | 0.7350 | $0.7310^{+0.0260}_{-0.0257}$ | 0.7339 | $0.7313^{+0.0197}_{-0.0207}$ | 0.7345 |
| Age/Gyr | $13.79^{+0.09}_{-0.08}$ | 13.78 | $13.78^{+0.08}_{-0.08}$ | 13.76 | $13.79^{+0.08}_{-0.08}$ | 13.76 |
| $\Omega_{\rm m}$ | $0.2706^{+0.0250}_{-0.0247}$ | 0.2650 | $0.2691^{+0.0257}_{-0.0260}$ | 0.2661 | $0.2687^{+0.0207}_{-0.0197}$ | 0.2654 |
| $z_{\rm re}$ | $10.40^{+1.14}_{-1.11}$ | 10.54 | $10.38^{+1.15}_{-1.12}$ | 10.48 | $10.27^{+0.72}_{-0.72}$ | 10.08 |
| $\rm H_0$ | $70.41^{+1.95}_{-1.96}$ | 70.77 | $70.58^{+2.02}_{-2.03}$ | 70.77 | $70.50^{+1.63}_{-1.65}$ | 70.83 |

**Table 8.** The constraints on the input and the derived parameters corresponding to the three different inflationary models arrived at upon using WMAP seven-year data. Note that the scalar amplitude $A_{\rm S}$ actually refers to the quantities $m^2$, $V_0$, and $\phi_*$ in the quadratic, the small field and the tachyon models, respectively.

| Model | Quadratic potential + step | | Small field model + step | | Tachyon model + step | |
|---|---|---|---|---|---|---|
| Parameters | Mean & 1-$\sigma$ | Best fit | Mean & 1-$\sigma$ | Best fit | Mean & 1-$\sigma$ | Best fit |
| $\Omega_{\rm b}\,h^2$ | $0.0224^{+0.0003}_{-0.0003}$ | 0.0224 | $0.0224^{+0.0003}_{-0.0003}$ | 0.0224 | $0.0224^{+0.0003}_{-0.0003}$ | 0.0224 |
| $\Omega_{\rm c}\,h^2$ | $0.1120^{+0.0051}_{-0.0050}$ | 0.1129 | $0.1118^{+0.0053}_{-0.0053}$ | 0.1128 | $0.1117^{+0.0042}_{-0.0041}$ | 0.1120 |
| $\theta$ | $1.039^{+0.002}_{-0.002}$ | 1.039 | $1.039^{+0.002}_{-0.002}$ | 1.040 | $1.039^{+0.002}_{-0.002}$ | 1.039 |
| $\tau$ | $0.0845^{+0.0056}_{-0.0060}$ | 0.0845 | $0.0857^{+0.0058}_{-0.0063}$ | 0.0842 | $0.0852^{+0.0042}_{-0.0042}$ | 0.0872 |
| $\ln\left[10^{10}\,A_{\rm S}\right]$ | $-0.6694^{+0.0309}_{-0.0318}$ | $-0.6644$ | $1.710^{+0.031}_{-0.031}$ | 1.714 | $34.509^{+0.003}_{-0.002}$ | 34.507 |
| $\alpha$ | $0.0015^{+0.0001}_{-0.0002}$ | 0.0016 | $0.1431^{+0.0033}_{-0.0030}$ | 0.1625 | $0.0016^{+0.0002}_{-0.0003}$ | 0.0015 |
| $\phi_0$ | $14.67^{+0.01}_{-0.01}$ | 14.67 | $7.887^{+0.00345}_{-0.0035}$ | 7.889 | $0.7820^{+0.0010}_{-0.0007}$ | 0.7810 |
| $\Delta\phi$ | $0.0249^{+0.0051}_{-0.0037}$ | 0.0258 | $0.0082^{+0.0018}_{-0.0014}$ | 0.0086 | $375.1^{+23.55}_{-23.17}$ | 366.9 |
| $\alpha/\Delta\phi$ | $0.0606^{+0.0098}_{-0.0094}$ | 0.0636 | $0.0179^{+0.0038}_{-0.0040}$ | 0.0189 | $0.4253^{+0.0540}_{-0.0545}$ | 0.4414 |
| $\Omega_\Lambda$ | $0.7252^{+0.0244}_{-0.0246}$ | 0.7214 | $0.7272^{+0.0254}_{-0.0251}$ | 0.7243 | $0.7272^{+0.0199}_{-0.0205}$ | 0.7265 |
| Age/Gyr | $13.80^{+0.08}_{-0.08}$ | 13.80 | $13.78^{+0.08}_{-0.08}$ | 13.78 | $13.79^{+0.08}_{-0.08}$ | 13.79 |
| $\Omega_{\rm m}$ | $0.2748^{+0.0246}_{-0.0244}$ | 0.2786 | $0.2728^{+0.0251}_{-0.0254}$ | 0.2757 | $0.2728^{+0.0205}_{-0.0200}$ | 0.2735 |
| $z_{\rm re}$ | $10.27^{+1.10}_{-1.12}$ | 10.33 | $10.37^{+1.10}_{-1.10}$ | 10.30 | $10.34^{+0.70}_{-0.71}$ | 10.53 |
| $\rm H_0$ | $70.07^{+1.88}_{-1.92}$ | 69.69 | $70.28^{+1.95}_{-1.93}$ | 70.02 | $70.22^{+1.58}_{-1.62}$ | 70.10 |

**Table 9.** The bounds on the background parameters and the parameters that describe the inflationary potentials and the step Eq. (9) obtained using the WMAP seven-year data. Note that the value of the height of the step $\alpha$ which has been quoted above for the small field and the tachyon models should be multiplied by $-10^{-3}$ and $-1$, respectively, while the location of the step $\phi_0$ should be multiplied by $10^6$ in the case of the tachyon model. Further, the values quoted for $(\alpha/\Delta\phi)$ should be multiplied by $-1$ in the case of the small field model, while it should be multiplied by $-10^{-5}$ in the case of the tachyon model.

the step, the second tachyon model Eq. (8) too exhibits a similar improvement in $\chi^2_{\rm eff}$. However, the model leads to a rather large red tilt and, therefore, in the absence of the step, it does not perform as well against the data as the other inflationary models that we have considered.

When we compare the contribution to the $\chi^2_{\rm eff}$ at the low multipoles (i.e. up to $\ell = 32$, see Refs. [1, 2]) from the output of the WMAP likelihood code for, say, the WMAP seven-year data, we find that the introduction of the step in the inflaton

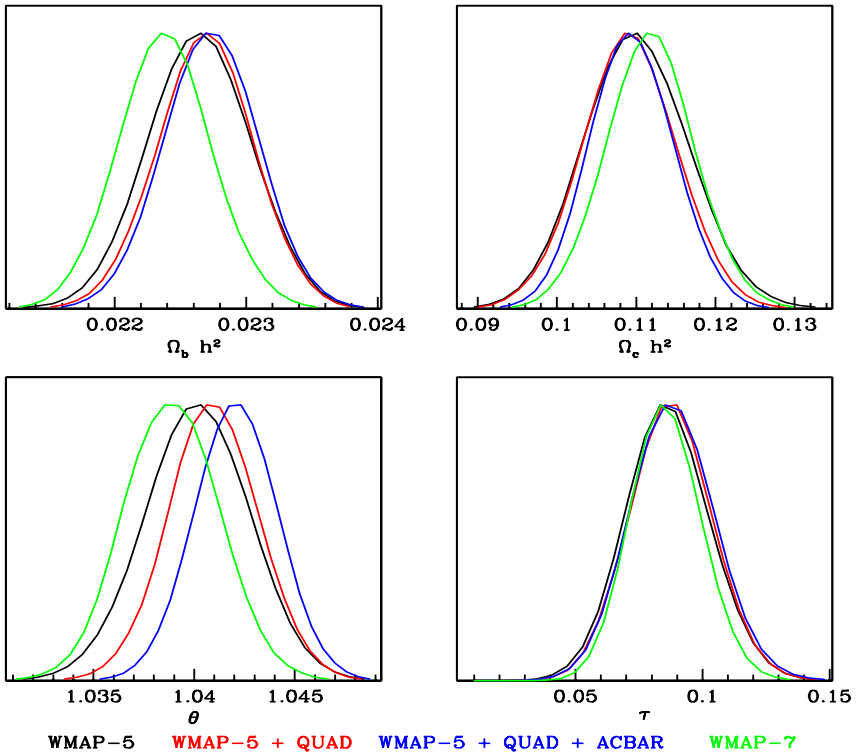


**Figure 1.** The one-dimensional likelihood distribution for the background parameters that we obtain in the case of the small field model with the step.

| Datasets / Models | WMAP-5 | WMAP-5 + QUaD | WMAP-5 + QUaD + ACBAR | WMAP-7 |
|---|---|---|---|---|
| Power law case | 2659.00 | 2758.36 | 2780.38 | 7474.81 |
| Quadratic potential | 2658.92 | 2758.22 | 2780.02 | 7474.78 |
| Quadratic potential + step | 2651.00 | 2750.33 | 2771.80 | 7466.16 |
| Small field model | 2658.87 | 2758.15 | 2779.99 | 7474.77 |
| Small field model + step | 2651.08 | 2750.50 | 2772.34 | 7466.07 |
| Tachyonic model | 2658.90 | 2758.22 | 2779.90 | 7474.78 |
| Tachyonic model + step | 2651.51 | 2751.27 | 2772.53 | 7465.88 |

**Table 10.** The $\chi^2_{\rm eff}$ for the different models and datasets that we have considered. Note that, as we had mentioned earlier, the Gibbs approach in the WMAP likelihood code has been used to calculate the $\chi^2_{\rm eff}$ for the CMB $TT$ spectrum at the low multipoles (i.e. for $\ell < 32$) [1, 2]. Without the step, all the inflationary models perform just as well as the power law case. And, evidently, the introduction of the step reduces $\chi^2_{\rm eff}$ by about 7-9 in *all* the cases.

potential reduces the $\chi^2_{\rm eff}$ for the $TT$ data over this range by about 5-6 in all the cases. In Figure 5, we have plotted the difference in $\chi^2_{\rm eff}$ with and without the step, as a function

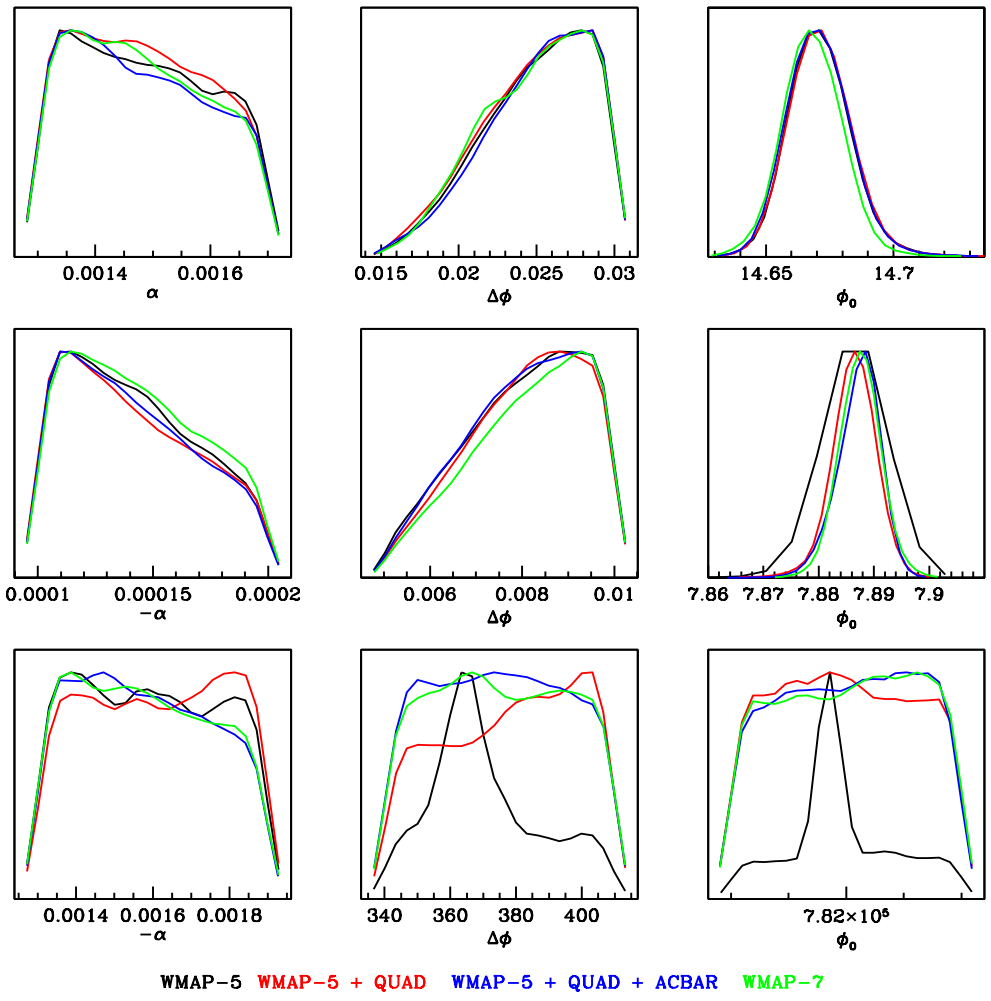


**Figure 2.** The one-dimensional likelihood distribution for the parameters describing the step in the three inflationary models of our interest. The top, middle and the bottom rows correspond to the quadratic potential, the small field model, and the tachyon model, respectively. Note that, for instance, the datasets strongly constrain the location of the step in both the canonical scalar field models. In contrast, the bounds are not equally tight on the height and the width of the step. In the case of the tachyon model, the constraints that we have arrived at seem prior dominated.

of the multipoles when $\ell > 32$, for the WMAP seven-year data. We have plotted the difference in $\chi^2_{\rm eff}$ for the cases of the quadratic potential and the small field model. It is clear from the figure that the additional improvement by about 2 arises due to a better fit near $\ell = 40$. (There also seems to be a 'loss' of about unity in $\chi^2_{\rm eff}$ at $\ell \lesssim 40$.) In other words, the step essentially improves the fit to the data at the lower multipoles. This point will be further evident in the following section, wherein we discuss the resulting the CMB angular power spectrum.

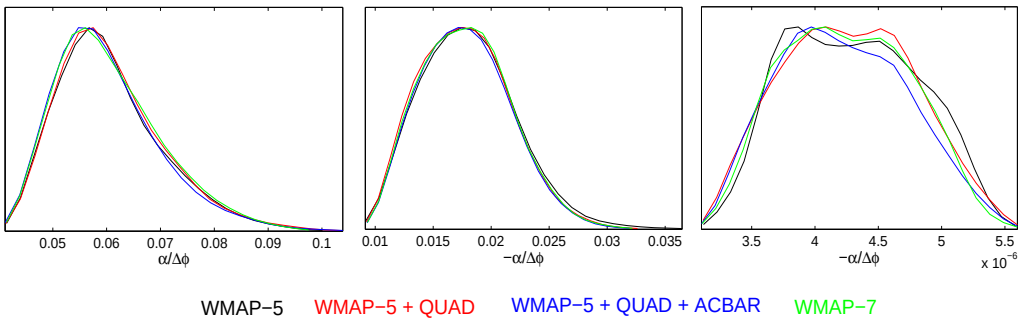


**Figure 3.** The one-dimensional likelihood distribution of the ratio of the height to the width of the step, viz. $(\alpha/\Delta\phi)$, for the three inflationary models that we have considered. The plots on the left, centre and the right correspond to the quadratic potential, the small field model, and the tachyon model, respectively. Clearly, while the datasets do not bound either the height or the width of the step well individually, they constrain the ratio of the two rather tightly.

## 5. The scalar and the CMB angular power spectra

As we had mentioned in the introductory section, the introduction of the step leads to a small deviation from slow roll inflation [9, 10]. We have illustrated this behavior in Figure 6, wherein we have plotted the evolution of the first two slow roll parameters $\epsilon$ and $\eta$ around the time when the field crosses the step (see, for instance, Refs. [17] and [14] for the definition of these slow roll parameters in the case of the canonical scalar field and the tachyon models, respectively). The small deviation from slow roll inflation leads to a burst of oscillations superimposed on the otherwise nearly scale invariant scalar power spectrum as we have illustrated in Figure 7. We should add that, since the deviation from slow roll is relatively small, the introduction of the step does not affect the tensor spectrum at all. It remains nearly scale invariant in all the cases. At the point $k = 0.05$ Mpc$^{-1}$, we find the tensor-to-scalar ratio $r$ to be about 0.16, 0.016 and 0.16 in the cases of the quadratic potential, the small field and the tachyon models, respectively.

The burst of oscillations in the scalar power spectrum in turn results in a feature in the CMB $TT$ angular power spectrum, which leads to the improvement in the fit to the data at the lower multipoles. This behavior is evident in Figure 8 wherein we have plotted the CMB $TT$ angular power spectra for the quadratic potential without and with the step, and for the small field model with the step. In Figure 9, we have plotted the corresponding $TE$ and $EE$ angular power spectra.

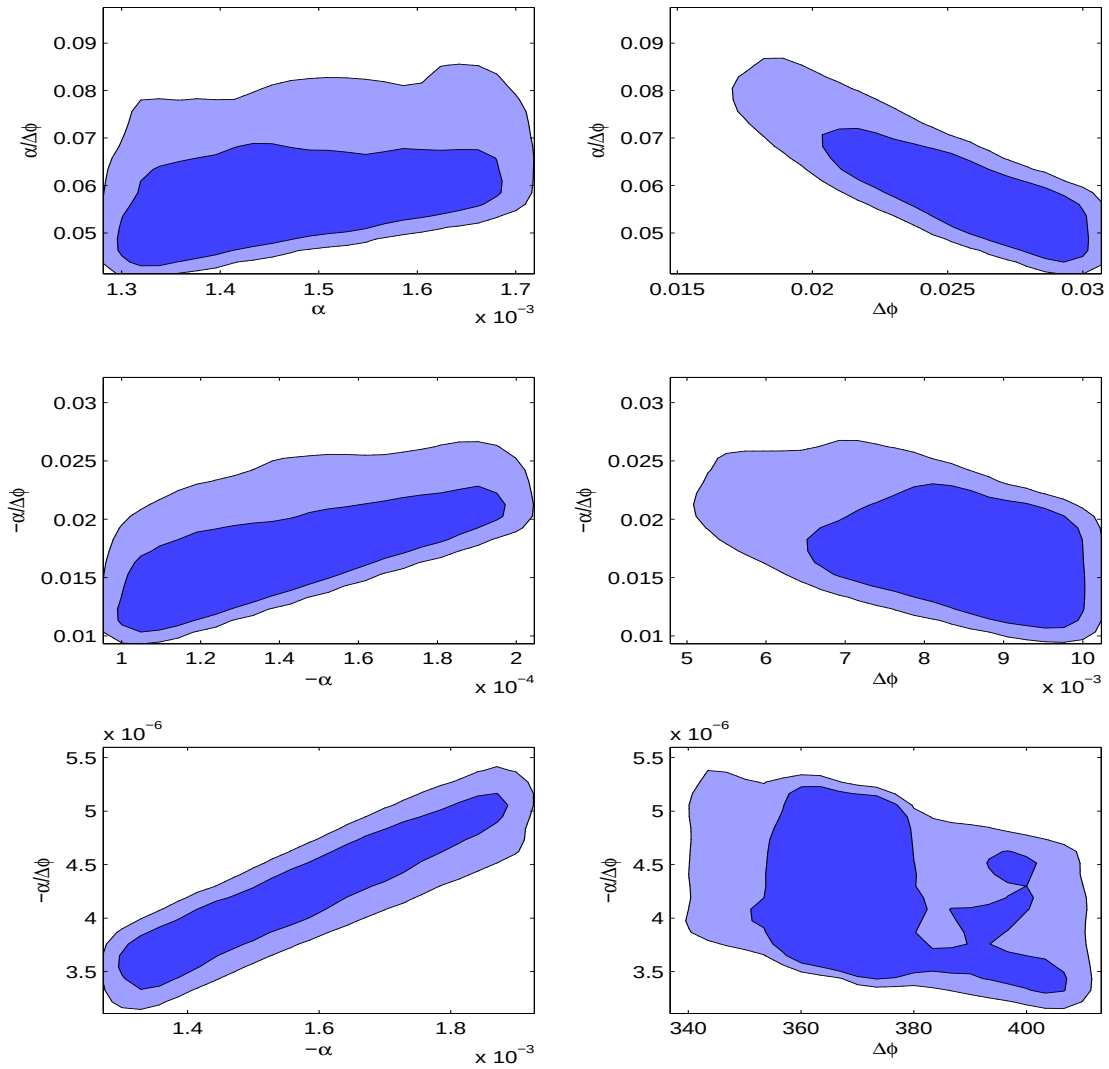


**Figure 4.** The joint two-dimensional likelihood distributions of the parameters $\alpha$ and $\Delta\phi$ with the slope $(\alpha/\Delta\phi)$, for the three inflationary models. These constraints are for the WMAP seven-year data. The top, middle and the bottom rows correspond to the quadratic potential, the small field model, and the tachyon model, respectively. These plots again point to the fact that, while the data does not bound either the height or the width of the step tightly, they constrain the ratio of the two rather well.

## 6. Summary and discussion

In this work, we have investigated the effects of introducing a step in certain inflationary models. In addition to revisiting the case of the quadratic potential that has been considered earlier, we have studied the effects of the step in a small field model and a tachyon model. The introduction of the step leads to a small deviation from slow roll inflation, which results in a burst of oscillations in the scalar power spectrum. These oscillations, in turn, leave their imprints as specific features in the CMB angular power spectrum. Actually, we have also evaluated the tensor power spectrum exactly, and

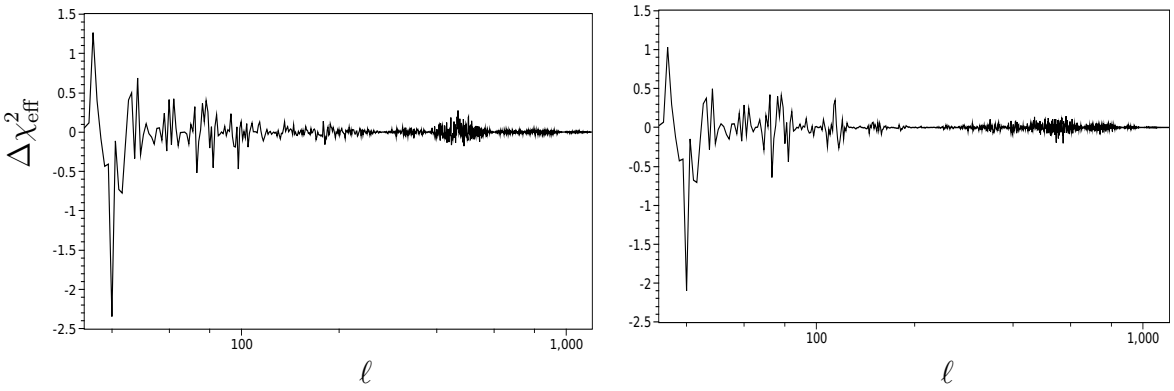


**Figure 5.** The difference in $\chi^2_{\rm eff}$ for the WMAP seven-year data with and without the step has been plotted as a function of the multipole moment for $\ell > 32$. The plot on the left corresponds to the quadratic potential, while the one on the right is for the small field model. The two figures are strikingly similar, and it is clear that the improvement in $\chi^2_{\rm eff}$ occurs near $\ell \simeq 40$ in both the cases. We find that the corresponding result for the tachyon model behaves in essentially the same fashion.

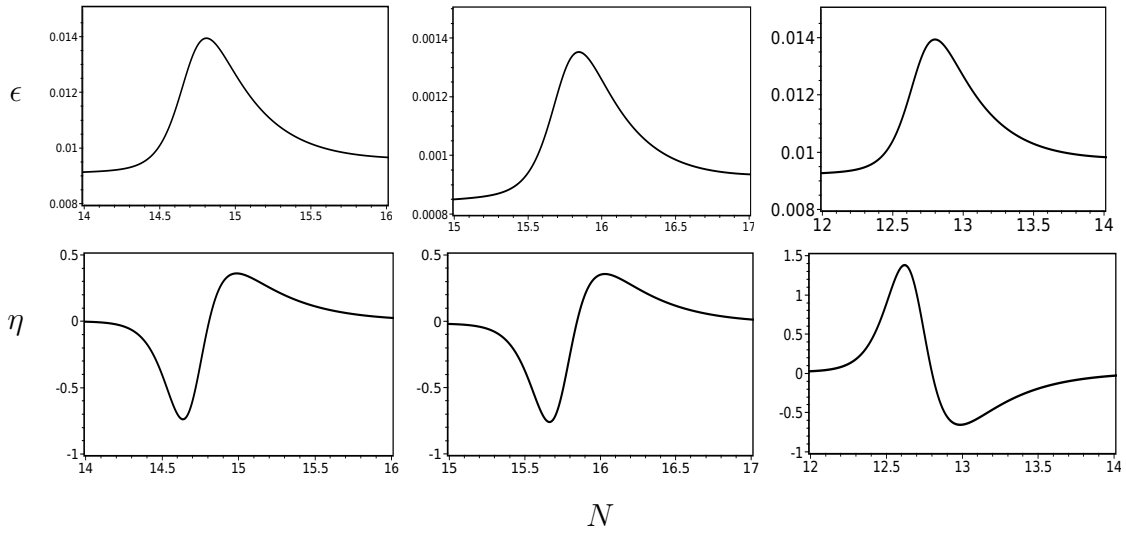


**Figure 6.** Typical evolution of the first two slow roll parameters $\epsilon$ and $\eta$ with the introduction of the step for the three inflationary models that we have considered. We have plotted the evolution of the slow roll parameters as a function of the e-folds $N$ for the quadratic potential (on the left), the small field model (in the middle), and the tachyon model (on the right), around the time when the field crosses the step in the potential.

have included it in our analysis. We believe that this is a timely effort considering the fact that results from, say, the ongoing PLANCK mission might necessitate such an analysis. Upon comparing the inflationary models with the WMAP, the QUaD and the ACBAR data, we find that, with the step, all the models lead to an improvement in $\chi^2_{\rm eff}$ by about 7-9 over the smooth, nearly scale invariant, slow roll spectrum, at the expense

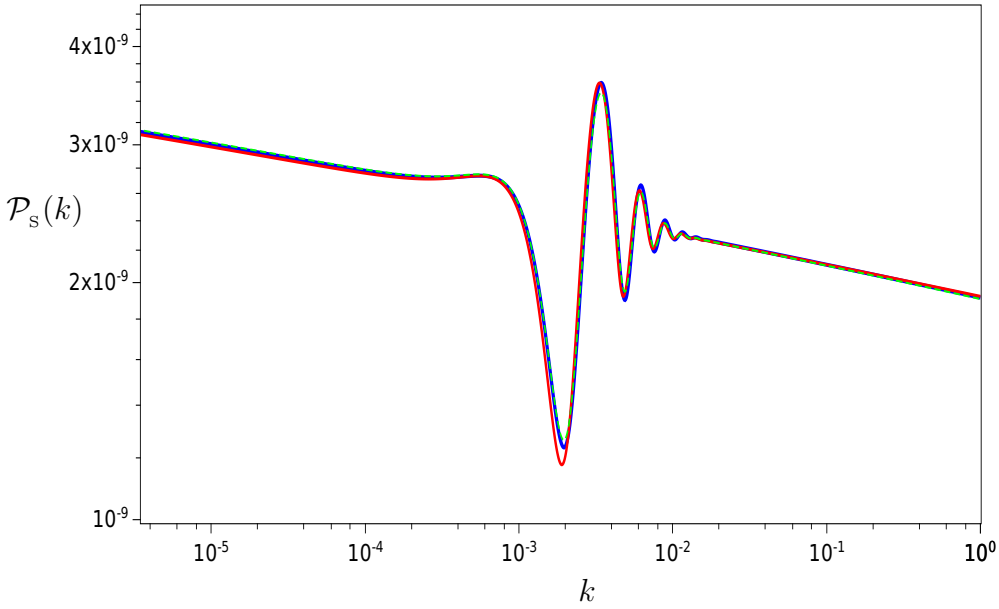


**Figure 7.** The scalar power spectra corresponding to the best fit values of the WMAP seven-year data for the inflationary models with the step. The solid blue, the solid red, and the dashed green curves describe the scalar power spectra in the cases of the quadratic potential, the small field model, and the tachyon model, respectively. Evidently, the three spectra are hardly distinguishable. And, obviously, the oscillations will not arise in the absence of the step.

of three additional parameters describing the location, the height and the width of the step in the inflaton potential. The output of the WMAP likelihood code and a plot of the difference in $\chi^2_{\rm eff}$ with and without the step clearly illustrate that the improvement occurs because of a better fit to the data at the lower multipoles due to the presence of the step. Evidently, if future observations indicate that the amplitude of the tensors are rather small, then the quadratic potential and the tachyon model will be ruled out, while a suitable small field model with a step can be expected to perform well against the data.

The introduction of step can possibly be viewed as an abrupt change in a potential parameter [8]. But, it has to be admitted that it is rather ad-hoc. It will be interesting to explore the generation of features and a resulting improvement in the fit in better motivated inflationary models. For instance, two field models with suitably chosen parameters can easily lead to a brief departure from slow roll inflation (in this context, see, for example, Refs. [11, 23, 24]). However, iso-curvature perturbations arise whenever more than one field is involved [25, 26], and they need to be carefully taken into account when comparing these models with the data. It will be a worthwhile effort to systematically explore the two field models, including the effects due to the iso-curvature perturbations, in an attempt to fit the outliers near the multipole moments of $\ell = 22$ and 40.

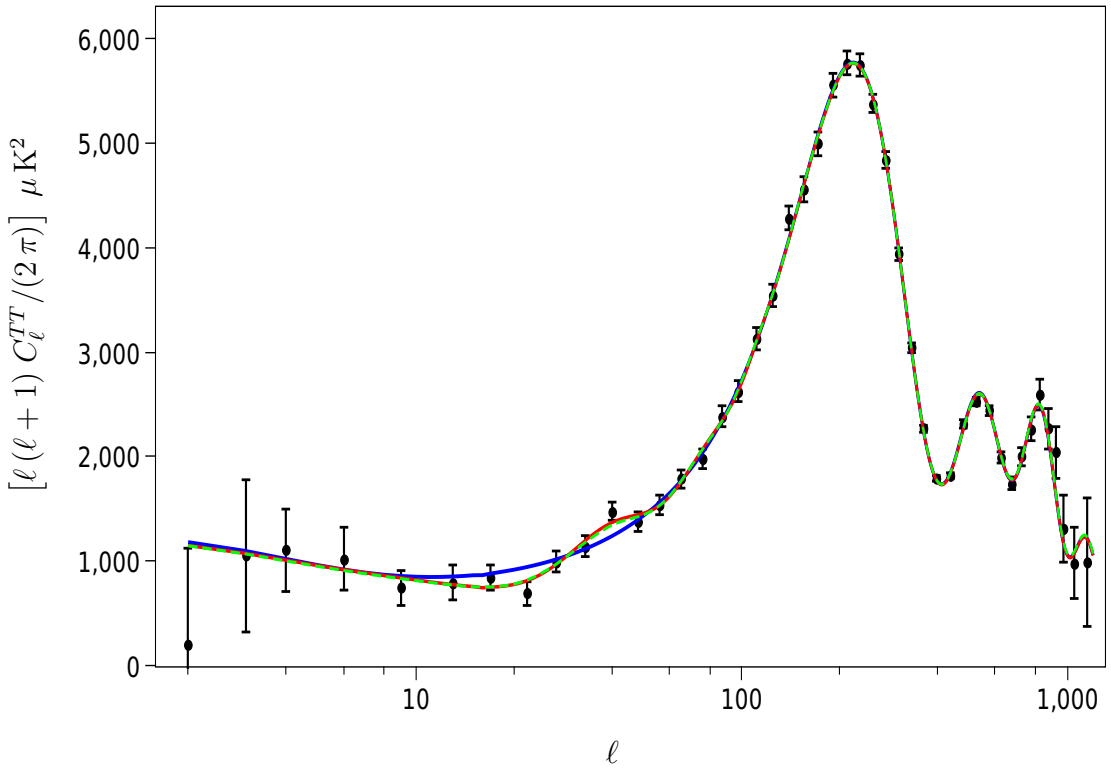


**Figure 8.** The CMB $TT$ angular power spectra corresponding to the best fit values of the inflationary models for the WMAP seven-year data without and with the step. The solid blue and the solid red curves correspond to the quadratic potential without and with the step, respectively. The dashed green curve corresponds to the best fit small field model with the step. We find that the results for the tachyon model behave in exactly the same fashion. The black dots with error bars denote the WMAP seven-year data. It is visually evident that, with the introduction of the step, the models lead to a better fit to the data near the multipole moments of $\ell = 22$ and 40.

Over the last few years, it has been recognized that primordial non-Gaussianity can act as a powerful observational tool that can help us discriminate further between the various inflationary models. For example, it is known that slow roll inflation driven by the canonical scalar fields leads only to a small amount of non-Gaussianity [27]. However, recent analysis of the CMB data seem to suggest that the extent of primordial non-Gaussianity may possibly be large (see, for instance, Refs. [2, 28]). It is known that models which lead to features, such as the ones we have considered here, also result in a reasonably large non-Gaussianity (see, for example, Refs. [29]). While the different models that we have considered in this work lead to virtually the same scalar power spectrum and almost the same extent of improvement in the fit (i.e. with the introduction of the step) to the CMB data, it is important to examine whether they lead to the same extent of non-Gaussianity as well. We are currently investigating such issues.

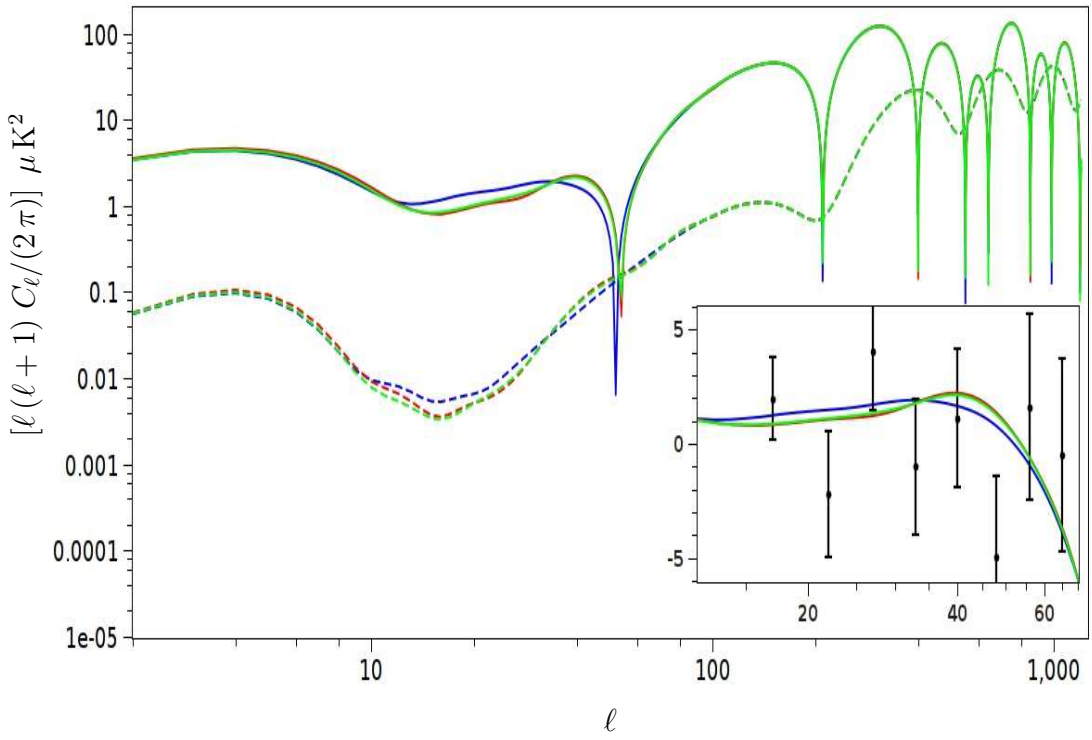


**Figure 9.** The CMB $TE$ and the $EE$ angular power spectra corresponding to the best fit values of the inflationary models for the WMAP seven-year data without and with the step. The solid blue, red and green curves represent the $TE$ spectrum (actually, its magnitude) for the quadratic potential without and with the step, and the small field model with the step, respectively. The dashed curves denote the corresponding $EE$ angular power spectra. The inset indicates the behavior of the $TE$ angular power spectra against the WMAP seven-year data over the multipole interval where the discrimination is maximal.

## Acknowledgments

We wish to thank Hiranya Peiris for extensive exchanges over e-mail on a few different issues related to the comparison of models with the data. RKJ and LS would like to thank Pravabati Chingangbam for discussions on related topics. DKH and LS would like to thank Jerome Martin for discussions. DKH also wishes to thank Sanjoy Biswas, Joydeep Chakrabortty, and Tirthankar Roy Choudhury for various help on numerical matters. MA would like to thank the Harish-Chandra Research Institute, Allahabad, India, for hospitality, where part of this work was carried out. We would also like to acknowledge the use of the high performance computing facilities at the Harish-Chandra Research Institute, Allahabad, India, as well as at the Inter-University Centre for Astronomy and Astrophysics, Pune, India. Finally, we acknowledge the use of the CosmoMC package [18], and the data products provided by the WMAP science team [22], the QUaD and the ACBAR missions.

## Appendix A. A few words on our code to evaluate the perturbation spectra

In this appendix, we shall rapidly outline the procedure we adopt to numerically evaluate the inflationary perturbation spectra, and also illustrate the accuracy of our numerical computation.

We evaluate the scalar and tensor power spectra numerically using a fast and accurate FORTRAN 90 code. The code is divided into two parts. The first part uses the fourth order Runge-Kutta algorithm [30] to solve the background equations for the scale factor and the scalar field, using e-folds as the independent variable. The background variables are evolved from some initial point in time until the point where the first slow roll parameter $\epsilon$ crosses unity. The initial values of the field and its velocity (i.e. $\phi$ and $\dot{\phi}$) are chosen by hand, and we ensure that the field starts in a slow roll phase. As is the standard practice, we choose the initial value of the scale factor such that the pivot scale (viz. $k = 0.05$ Mpc$^{-1}$) leaves the Hubble radius at 50 e-folds before the end of the inflation [9, 10].

The second part of the code uses the Bulirsch-Stoer algorithm [30] to evolve the perturbations. We impose the standard Bunch-Davies initial conditions on the perturbations. As is usually done [8, 31, 32], the initial conditions on the modes are imposed when they are well inside the Hubble radius [say, when $k = (100\, a\, H)$]. The modes are evolved until they are sufficiently outside the Hubble radius and the curvature perturbation reaches its asymptotic value [typically, this occurs when $k \simeq (10^{-5}\, a\, H)$]. The tensor perturbations are evolved in a similar fashion. We should mention here that, while the speed of propagation of the curvature perturbations induced by the canonical scalar field is a constant (and, equal to unity), it changes with time in the case of the tachyon models [14, 33]. We have carefully taken this point into account, while imposing the initial conditions on the modes as well as when evolving them from the sub-Hubble to the super-Hubble scales.

We then couple our code to the publicly available cosmological Boltzmann code CAMB [20, 21] to calculate the angular power spectra of the CMB anisotropies. We evaluate the scalar and the tensor spectra for all the modes that are required by CAMB to arrive at the CMB angular power spectra.

To check the accuracy of the FORTRAN code, we have compared each code with the same code having a much smaller step size. The check has also allowed us to optimize the code. We have also compared our results (for the background as well as the perturbations) with the results from Mathematica [34], where the differential equations are solved with very high accuracy. We have included below the plots of the power spectra in a couple of different cases that were obtained using the FORTRAN 90 and the Mathematica codes. The various checks we have carried out indicate that the FORTRAN code we have used is always accurate to better than 0.1%.

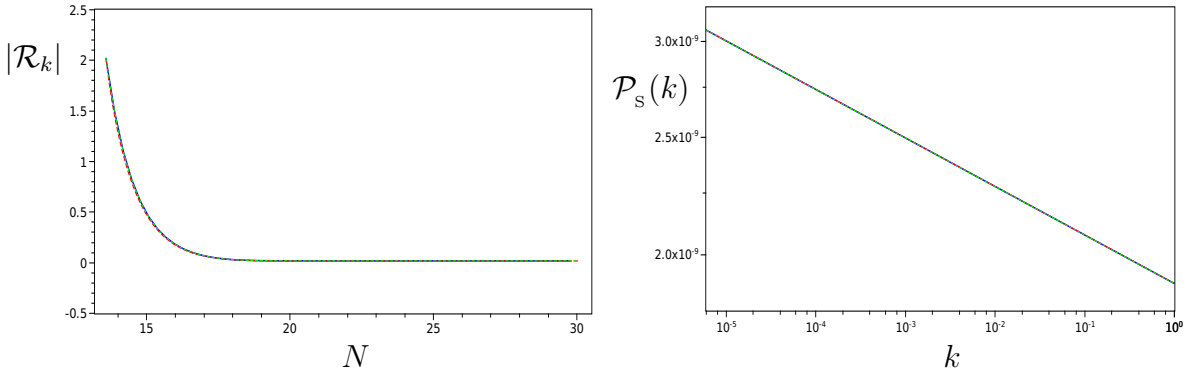


**Figure A1.** On the left, we have plotted the evolution of the amplitude of the curvature perturbation $\mathcal{R}_k$ in power law inflation as a function of the number of e-folds $N$, for the pivot scale. The figure on the right contains the scalar spectrum in power law inflation. In these plots, the solid blue lines represent the analytical results that are available in the case of power law inflation, while the solid red lines and the dashed green lines denote the results from the FORTRAN and the Mathematica codes, respectively. The different colors in the plots are not clearly visible since the curves fall right on top of each other. Actually, we find that these results match each other to better than an accuracy of 0.1%.

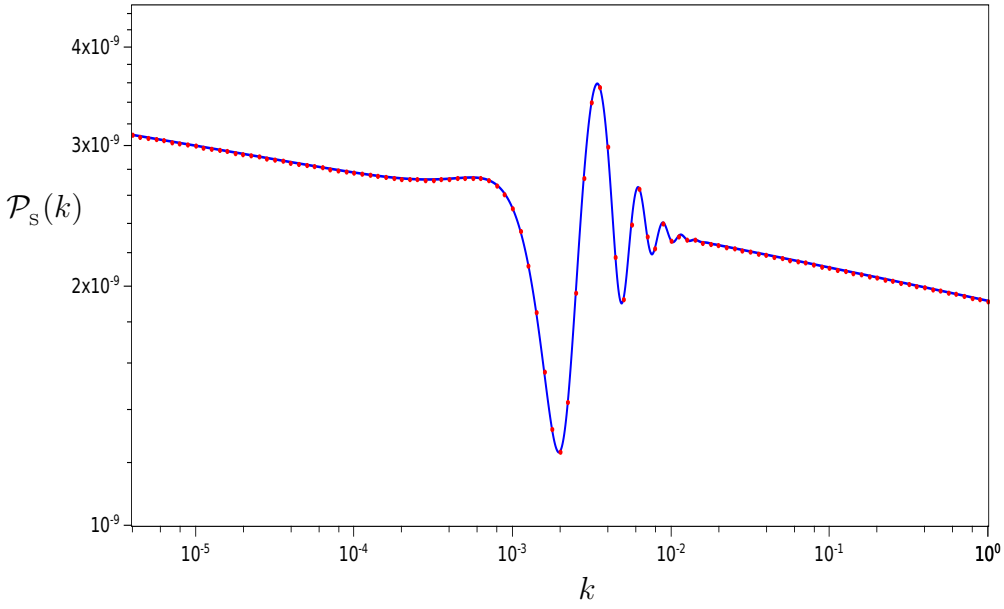


**Figure A2.** The scalar power spectrum from the FORTRAN (as the solid blue line) and the Mathematica (as red dots) codes have been plotted for the best fit quadratic potential with the step. The two power spectra match each other to an accuracy better than 0.1%.

## References

[1] J. Dunkley *et al.*, Astrophys. J. Suppl. **180**, 306 (2009); E. Komatsu *et al.*, Astrophys. J. Suppl. **180**, 330 (2009).

[2] D. Larson *et al.*, arXiv:1001.4635v1 [astro-ph.CO]; E. Komatsu *et al.*, arXiv:1001.4538v2 [astro-ph.CO].
[3] M. L. Brown *et al.*, Astrophys. J. **705**, 978 (2009).
[4] C. L. Reichardt *et al.*, Astrophys. J. **694**, 1200 (2009).
[5] S. Hannestad, Phys. Rev. D **63**, 043009 (2001); S. L. Bridle, A. M. Lewis, J. Weller and G. Efstathiou, Mon. Not. Roy. Astron. Soc. **342**, L72 (2003); P. Mukherjee and Y. Wang, Astrophys. J. **599**, 1 (2003); S. Hannestad, JCAP **0404**, 002 (2004); A. Shafieloo and T. Souradeep, Phys. Rev. D **70**, 043523 (2004); D. Tocchini-Valentini, Y. Hoffman and J. Silk, Mon. Not. Roy. Astron. Soc. **367**, 1095 (2006); A. Shafieloo, T. Souradeep, P. Manimaran, P. K. Panigrahi and R. Rangarajan, Phys. Rev. D **75**, 123502 (2007); A. Shafieloo and T. Souradeep, Phys. Rev. D **78**, 023511 (2008); R. Nagata and J. Yokoyama, Phys. Rev. D **79**, 043010 (2009); G. Nicholson and C. R. Contaldi, JCAP **0907**, 011 (2009).
[6] A. A. Starobinsky, Sov. Phys. JETP Lett. **55**, 489 (1992).
[7] C. Dvorkin and W. Hu, Phys. Rev. D **81**, 023518 (2010).
[8] J. A. Adams, B. Cresswell and R. Easther, Phys. Rev. D **64**, 123514 (2001).
[9] L. Covi, J. Hamann, A. Melchiorri, A. Slosar and I. Sorbera, Phys. Rev. D **74**, 083509 (2006); J. Hamann, L. Covi, A. Melchiorri and A. Slosar, Phys. Rev. D **76**, 023503 (2007).
[10] M. J. Mortonson, C. Dvorkin, H. V. Peiris and W. Hu, Phys. Rev. D **79**, 103519 (2009).
[11] M. Joy, V. Sahni, A. A. Starobinsky, Phys. Rev. D **77**, 023514 (2008); M. Joy, A. Shafieloo, V. Sahni, A. A. Starobinsky, JCAP **0906**, 028 (2009).
[12] R. K. Jain, P. Chingangbam, J.-O. Gong, L. Sriramkumar and T. Souradeep, JCAP **0901**, 009 (2009); R. K. Jain, P. Chingangbam, L. Sriramkumar and T. Souradeep, arXiv:0904.2518v1 [astro-ph.CO].
[13] G. Efstathiou and S. Chongchitnan, Prog. Theor. Phys. Suppl. **163**, 204 (2006).
[14] D. A. Steer and F. Vernizzi, Phys. Rev. D **70**, 043527 (2004).
[15] See, `http://www.sciops.esa.int/PLANCK/`.
[16] B. Bassett, S. Tsujikawa and D. Wands, Rev. Mod. Phys. **78**, 537 (2006).
[17] L. Sriramkumar, Curr. Sci. **97**, 868 (2009).
[18] See, `http://cosmologist.info/cosmomc/`.
[19] A. Lewis and S. Bridle, Phys. Rev. D **66**, 103511 (2002).
[20] A. Lewis, A. Challinor and A. Lasenby, Astrophys. J. **538**, 473 (2000).
[21] See, `http://camb.info/`.
[22] See, `http://lambda.gsfc.nasa.gov/`.
[23] J. M. Cline, P. Crotty and J. Lesgourgues, JCAP **0309**, 010 (2003).
[24] P. Hunt and S. Sarkar, Phys. Rev. D **70**, 103518 (2004); Phys. Rev. D **76**, 123504 (2007).
[25] C. Gordon, D. Wands, B. A. Bassett and R. Maartens, Phys. Rev. D **63**, 023506 (2000).
[26] S. Tsujikawa, D. Parkinson and B. A. Bassett, Phys. Rev. D **67**, 083516 (2003); D. Parkinson, S. Tsujikawa and B. A. Bassett, Phys. Rev. D **71**, 063524 (2005).
[27] J. Maldacena, JHEP **0305**, 013 (2003).
[28] K. M. Smith, L. Senatore and M. Zaldarriaga, JCAP **0909**, 006 (2009).
[29] X. Chen, R. Easther and E. A. Lim, JCAP **0706**, 023 (2007); JCAP **0804**, 010 (2008)
[30] W. H. Press, S. A. Teukolsky, W. T. Vetterling and B. P. Flannery, *Numerical Recipes in FORTRAN 90*, Second edition (Cambridge University Press, Cambridge, England, 1996).
[31] D. S. Salopek, J. R. Bond and J. M. Bardeen, Phys. Rev. D **40**, 1753 (1989).
[32] C. Ringeval, Lect. Notes Phys. **738**, 243 (2008).
[33] R. K. Jain, P. Chingangbam and L. Sriramkumar, JCAP **0710**, 003 (2007).
[34] See, `http://www.wolfram.com/`.